www.MaterialsViews.com

Nanowires

A Nonconventional Approach to Patterned Nanoarrays of DNA Strands for Template-Assisted Assembly of Polyfluorene Nanowires

Dong Geun Bae, Ji-Eun Jeong, Seok Hee Kang, Myunghwan Byun, Dong-Wook Han, Zhiqun Lin, Han Young Woo, and Suck Won Hong**

DNA molecules have been widely recognized as promising building blocks for constructing functional nanostructures with two main features, that is, self-assembly and rich chemical functionality. The intrinsic feature size of DNA makes it attractive for creating versatile nanostructures. Moreover, the ease of access to tune the surface of DNA by chemical functionalization offers numerous opportunities for many applications. Herein, a simple yet robust strategy is developed to yield the self-assembly of DNA by exploiting controlled evaporative assembly of DNA solution in a unique confined geometry. Intriguingly, depending on the concentration of DNA solution, highly aligned nanostructured fibrillar-like arrays and well-positioned concentric ring-like superstructures composed of DNAs are formed. Subsequently, the ring-like negatively charged DNA superstructures are employed as template to produce conductive organic nanowires on a silicon substrate by complexing with a positively charged conjugated polyelectrolyte poly[9,9-bis(6′-N,N,N-trimethylammoniumhexyl) fluorene dibromide] (PF2) through the strong electrostatic interaction. Finally, a monolithic integration of aligned arrays of DNA-templated PF2 nanowires to yield two DNA/PF2-based devices is demonstrated. It is envisioned that this strategy can be readily extended to pattern other biomolecules and may render a broad range of potential applications from the nucleotide sequence and hybridization as recognition events to transducing elements in chemical sensors.

D. G. Bae, S. H. Kang, Prof. D.-W. Han, Prof. S. W. Hong
Department of Cogno-Mechatronics Engineering
Department of Optics and Mechatronics Engineering
Pusan National University
Busan 609-735, Republic of Korea
E-mail: swhong@pusan.ac.kr

J.-E. Jeong, Prof. H. Y. Woo
Department of Chemistry
Korea University
Seoul 136-713, Republic of Korea
E-mail: hywoo@korea.ac.kr

Prof. M. Byun
Department of Advanced Materials Engineering
Keimyung University
Daegu 704-701, Republic of Korea

Prof. Z. Lin
School of Materials Science and Engineering
Georgia Institute of Technology
Atlanta, GA 30332, USA

DOI: 10.1002/smll.201601346

small NANO MICRO

1. Introduction

Many biological molecules are known to self-assemble into ordered and complex structures using their selective molecular recognition properties.[1] Intermolecular self-assembly programmed by molecular recognition events that are dynamically driven by energy dissipation has been recognized as the spontaneous process of molecules. This enables to build spatially defined molecular architectures from the nanoscale to macroscopic dimensions.[2–4] DNA have been capitalized on as a structural material to arrange organic and inorganic molecular components using DNA as a template has been demonstrated.[5–8] DNA self-assembly has attracted significant attention as it offers a bottom-up manufacturing technique to provide efficient templates for the subsequent assembly of either organic or inorganic nanoelements such as metallic charged nanoparticles or streptavidin proteins.[9–12] Surface modification of individual DNAs and their configurations is of crucial importance to develop nanoscale devices based on DNA-templated assembly.[13,14] In this context, the specific immobilization of a large number of DNA molecules on a solid substrate has progressed over the past years for many potential applications such as electronic, magnetic, optoelectronic, and sensors, in which DNA molecules are "addressable" only when they are highly ordered or stretched. Moreover, sufficient mechanical rigidity, rich chemical functionality, and the programmable structures of DNA provide opportunities to construct 1D and 2D templates such as nanowires, ribbons, nanotubes, and nanotiles,[4,9] while retaining its structural integrity under the mild reaction conditions in order to form metals, semiconductors, or conductive polymers.[15,16]

In order to form the efficient DNA assembly by stretching and organization, the moving meniscus of DNA solutions has offered a wide variety of combing-based means to elongate and fix DNA molecules on substrates. For instance, a natural drying process (i.e., drop casting), spin-stretching on a spinning disk, Langmuir–Blodgett technique, flowing DNA solutions on the air/liquid interface in microfluidic channels, and electrophoresis separation have been demonstrated to form well-defined shapes and arrays of DNA molecules.[17–21] These results suggested the possibilities of precise control of the orientation and curvature of DNA molecules, although DNA was still randomly distributed with a significant number of unwanted defects, which restricted the development of device arrays. Moreover, a soft lithography method was applied to realize the highly effective periodic alignment of DNA via a polydimethylsiloxane stamp assisted molecular combing process.[22,23] However, the use of a lithographic method often requires expensive equipment and multistep procedures. Clearly, a cost-effective strategy for organizing DNA molecules at large length scale still remains challenging.

Recently, highly regular self-organized concentric arrays composed of polymers, nanoparticles, single-walled carbon nanotubes, etc., have been reported by allowing a drop of solution containing nonvolatile solutes noted above to evaporate in a constrained geometry comprising a spherical lens on a flat substrate.[24–27] With such a geometric confinement, the maximum evaporative loss of solvent via evaporation is induced only at the edge of evaporating solution instead of the entire droplet surface as in the conventional approaches which yields coffee ring-like stains.[28] Within a certain concentration regime, a number of concentric ring patterns are spontaneously formed by controlled, repetitive pinning and depinning events of the contact line (i.e., "stick–slip" motion).[29] This dynamic motion due to the evaporative loss of solvent leads to the formation of patterned films where the solute lines are deposited during a "stick" event and the spacing is dictated by the "slip" of the meniscus which are governed by the competition between the capillary force and the pinning force.[25] Therefore, it is essential to control the evaporation flux, the solution concentration, and the interfacial interaction between the solute and substrate for fine-tuning the ordered structures.[30–32]

Herein, we report a simple yet facile technique to craft a set of intriguing patterns composed of salmon sperm DNA (≈2000 bp, Sigma-Aldrich) from the drying-mediated self-assembly in a confined geometry where the DNA solution is held by capillary force. The straight DNA bundles, curled structure, and concentric ring patterns were created by varying the DNA solution concentration. In particular, periodically spaced concentric line patterns of DNA strands with unprecedented regularity over large area were produced. In order to engineer these self-organized DNA structures for their integration into electronic devices, the surface modification is essential due to the poor electrical characteristics of DNA. To this end, a cationic conjugated polyelectrolyte (CPE), poly[9,9-bis(6′-*N,N,N*-trimethylammoniumhexyl)fluorene dibromide] (PF2) was used to form a complex with DNA in aqueous solution.[33,34] The complexation of cationic PF2 with anionic biological polyelectrolytes (i.e., salmon sperm DNA) offers an effective means of building the patterned structures of semiconducting conjugated polymers. The current–voltage characteristics of patterned DNA and DNA/PF2 complex structures were investigated. PF2 carries the advantage of mechanical flexibility and chemical similarity, which enables not only the fabrication of well-organized arrays of a biological polyelectrolyte in a controllable manner but also the functionalization of biomolecules with electrostatic complementarity of CPE and DNA.[33,35,16] As such, this preparative strategy may suggest a viable route to incorporating biomolecules and semiconducting organic materials into the highly organized patterns for potential applications in surface-bound biosensors, bioelectronic devices, etc.[34,36,37,16]

2. Results and Discussion

2.1. Drying-Mediated Assembly of DNA Strands in Sphere-On-Flat Geometry

A schematic illustration of a droplet of salmon sperm DNA (hereafter referred to as DNA) solution loaded in a confined geometry consisting of a spherical lens on a Si/SiO_2 substrate (i.e., a sphere-on-flat geometry) is shown in **Figure 1**a. The two surfaces are initially separated by a few hundred micrometers apart using a micropositioning stage with a lens holder,

www.MaterialsViews.com

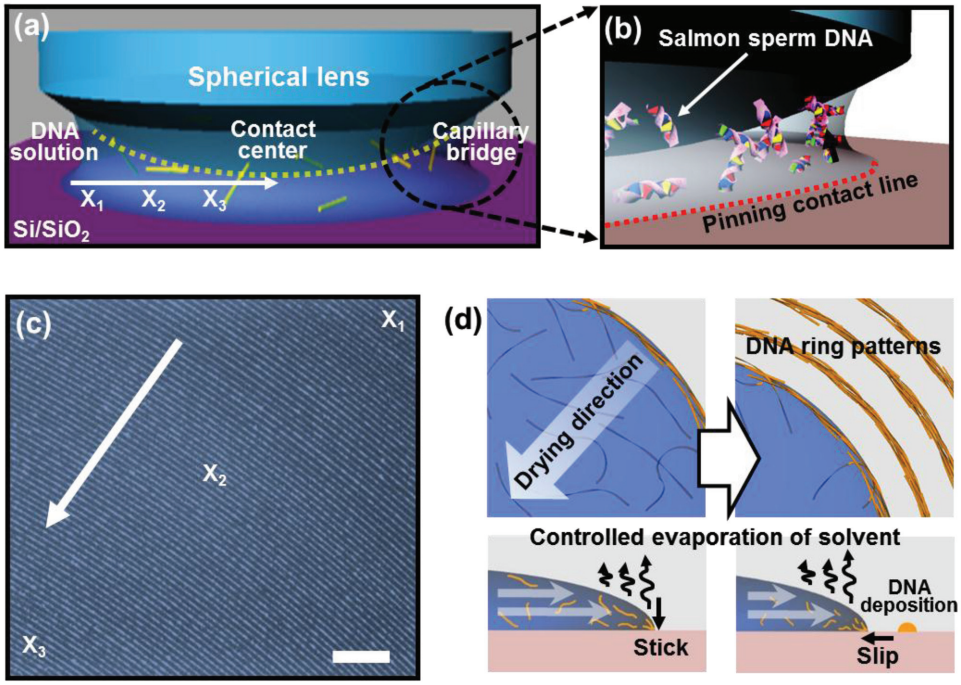

Figure 1. a) Schematic illustration of the sphere-on-flat geometry: cross-sectional view of a capillary-held DNA solution placed in a capillary bridge, where X_n ($n = 1–3$) indicates the radial position away from the contact center. b) Close-up, cross-sectional view of the right capillary edge forming an initial pinning contact line (dashed line). c) Representative optical microscopy images of highly regular concentric DNA-ring patterns over large area obtained from drying-mediated self-assembly with 50 μg mL^{-1} DNA aqueous solution in the confined geometry (a). The arrow on the left marks the moving direction of the solution front during the course of evaporation. X_1, X_2, and X_3 are the distances of ring away from the sphere/substrate contact center at outermost region (X_1), intermediate region (X_2), and innermost region (X_3), respectively. Scale bar = 150 μm. d) Schematic representation of the stepwise formation of DNA rings (upper panels) via a controlled evaporation of solvent at the edge of a DNA droplet and repetitive "stick-slip" motion of the contact line (lower panels).

and then the aqueous DNA droplet was loaded in between the two surfaces. Next, the upper spherical lens was slowly brought into contact with the lower Si/SiO_2 substrate such that a capillary-held DNA solution forms with the highest evaporation rate only at the edge of a solution.[25,26] Consequently, an initial circular pinning contact line was exerted (a red dashed line in Figure 1b). During the course of solvent evaporation in a sealed chamber, cyclic stick–slip motions of the three-phase contact line were preceded until the solvent was completely dried out; the circular-shaped pinning contact line gradually moved toward the center of the sphere–substrate contact (contact center, Figure 1a). Afterward, the two surfaces were carefully separated and the formed patterned structures on the substrate were examined by an optical microscope. Shown in Figure 1c is a representative optical micrograph of the remarkably regular concentric DNA ring patterns over a lateral distance of millimeter scale obtained by the deposition of DNAs from 50 μg mL^{-1} DNA water solution. The formation of periodic patterns can be understood as a direct consequence of controlled, repetitive stick–slip motions of receding contact lines as illustrated in Figure 1d. The consecutive motions of the contact line are governed by the balance between pinning (i.e., mainly reflected by the friction force) and depinning forces (i.e., the capillary force caused by the surface tension of solvent) at the liquid/substrate interface.[38] The assembly of DNA strands also depends on many factors such as solution concentration, solvent evaporation rate, and solute/substrate interactions. Most of all, however, we postulate a periodic temporal-spatial variation of DNA concentration in the receding meniscus should play an important role in pattern formation where the local change in concentration of solution drop leads to periodic deposition on the substrate.[32] During the drying process, an outward flow of solution diffuses from the bulk solution to replenish the highest evaporation loss at the extremity of a solution, which also transports DNA molecules from the bulk solution (Figure 1d, left panels). Therefore, the local concentration in the meniscus becomes increasingly higher. When it reaches a certain threshold value, DNA molecules begin to form densely packed aggregates on the substrate.[39] Therefore, more DNA molecules can be continuously precipitated and jammed on the substrate. In the meantime, the meniscus is shrunk forming concave curvature, and the initial contact angle at the edge of contact line decreased via continuous solvent evaporation, at which the depinning force exceeds the pinning force. When the contact angle becomes smaller than the critical contact angle, the contact line moves quickly inward, and thus a new position develops (Figure 1d, right lower panel).[38] Meanwhile, the solution recovers the initial DNA concentration again and the continuous cyclic pinning–depinning process regularly repeats until it moves into the sphere/Si contact center. It is noteworthy that this simple sphere-on-flat geometry facilitates the suppression of hydrodynamic instabilities, and thus providing a precisely controlled environment for the solvent evaporation,[24–27,30] compared to single-droplet drying approaches.[28,29]

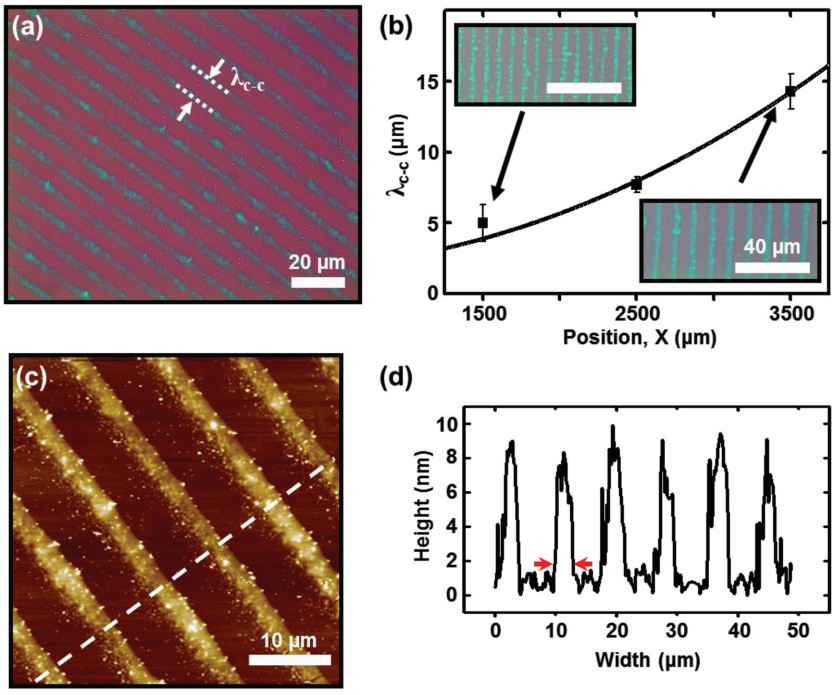

Figure 2. a) Optical micrograph of a small zone of highly ordered DNA rings on Si/SiO_2 substrate (locally, they appeared as parallel straight stripes) at intermediate region, X_2 in Figure 1c (c = 50 μg mL^{-1}). DNA stripes were formed perpendicular to the moving direction of solution front. Center-to-center distance between the DNA stripes is marked as $\lambda_{C\text{-}C}$. Scale bar = 20 μm. b) Gradient periodic DNA-stripe pattern formation; $\lambda_{C\text{-}C}$ values are plotted as a function of X, where X is the distance from the sphere/substrate contact center. Two representative optical microscopy images are given as insets. Scale bar = 40 μm. c) A typical AFM height image of DNA stripes on Si/SiO_2 substrate. Scale bar = 10 μm. d) The corresponding AFM height profile taken along the direction marked by the dashed line in (c).

Figure 2 summarizes the details about the highly ordered DNA ring patterns formed by the controlled evaporation in the sphere-on-flat geometry. Figure 2a represents a highly magnified optical micrograph of DNA ring patterns created from the 50 μg mL^{-1} solution; locally, it shows extremely regular periodic striped patterns, with no residual DNA strands between the adjacent stripes, where the deposited stripes are parallel to the receding contact line and have typical distances noted as $\lambda_{C\text{-}C}$ (the center-to-center distance of the stripes, marked in Figure 2a). In Figure 2b, the experimental results show that the trend of a "jumping distance" $\lambda_{C\text{-}C}$ between consecutive stripe patterns increases with increasing distance from the contact center. The inset images at the different radial distance away from the center of sphere/flat substrate contact (noted X_1, X_2, and X_3 in Figure 1a,c) show different densities of DNA stripes in the same observed area. It has been investigated that the origin of this gradient fashion (the rate of change of $\lambda_{C\text{-}C}$) is expected to be due to a delicate interplay of the geometrical constraint (i.e., the surface profile of the spherical lens).[38] To explore the surface morphology of parallel stripe patterns of DNA shown in Figure 2a, atomic force microscope (AFM) measurements were performed (Figure 2c). It reveals that several microns wide and several nanometers high DNA stripes were formed with high regularity and fidelity. Figure 2d shows the surface profiling of micro-patterned DNA; the average height, H_{ring}, was measured to be 9.1 ± 0.5 nm corresponding to several stacking layers of dsDNA molecules and the average width of patterns, W_{ring}, was measured to be 4.2 ± 0.4 μm, respectively.

2.2. Effects of DNA Concentration on Morphological Changes of DNA Patterns

A range of different intriguing surface patterns were crafted by varying the droplet concentrations. In the present study, as shown in **Figure 3**, gradual but clear morphological changes were observed with decreasing the DNA concentration from 1000 to 10 μg mL^{-1}. As for the concentration as high as 1000 μg mL^{-1}, the assembled DNA pattern was not of a ring pattern horizontally to the contact line (Figure 2) but of a textured film that covers the axially symmetric sphere-on-flat geometry (Figure 3a), so-called spoke-like structures. The local orientation of DNA assemblies within this concentration regime was very uniform with nematic-like ordering of densely packed straight DNA bundles over the entire macroscopic areas as shown in Figure 3a; optical microscopic image shows that the DNA strands were "woven" into ordered fibril bundles parallel to the drying direction (i.e., molecular combing of DNA).[19,40] Notably, the individual DNA filaments were firmly tethered on a flat surface with highly uniform orientation toward the contact center (i.e., radial spokes) without positional ordering as a result of intermolecular condensation during the drying process. Analogous to the aligning deposition process of other small molecules such as nanoparticles[41] or carbon nanotubes,[42] the formation of DNA spokes can be easily understood as follows. At the early stage of the deposition process, when a sufficiently concentrated DNA solution was provided in confined geometry, a large number of DNAs were precipitated and supersaturated at the pinned contact line on the substrate. These anchored DNAs initially served as nucleation sites and grew into DNA bundles that are aligned perpendicular to the contact line by continuously replenished DNA solutes from the interior solution. Hence, the DNA molecules were straightened and condensed at the same time due to the lateral evaporation-induced capillary force acting on the length direction of DNA molecules at the receding solution front during the successive drying of the liquid film. This resulted in highly packed spoke patterns. It is worth noting that this type of long-range textured DNA structures were created only by confining the drying process within geometries (Figure S1, Supporting Information); on a flat single surface, the dispersion readily wets and large aggregates of DNAs were found to be randomly distributed. Interestingly, at the inner-most site (denoted as X_3 in Figure 1a), the deposited DNA bundles exhibited alternating slightly jammed and regularly elongated DNA bundle

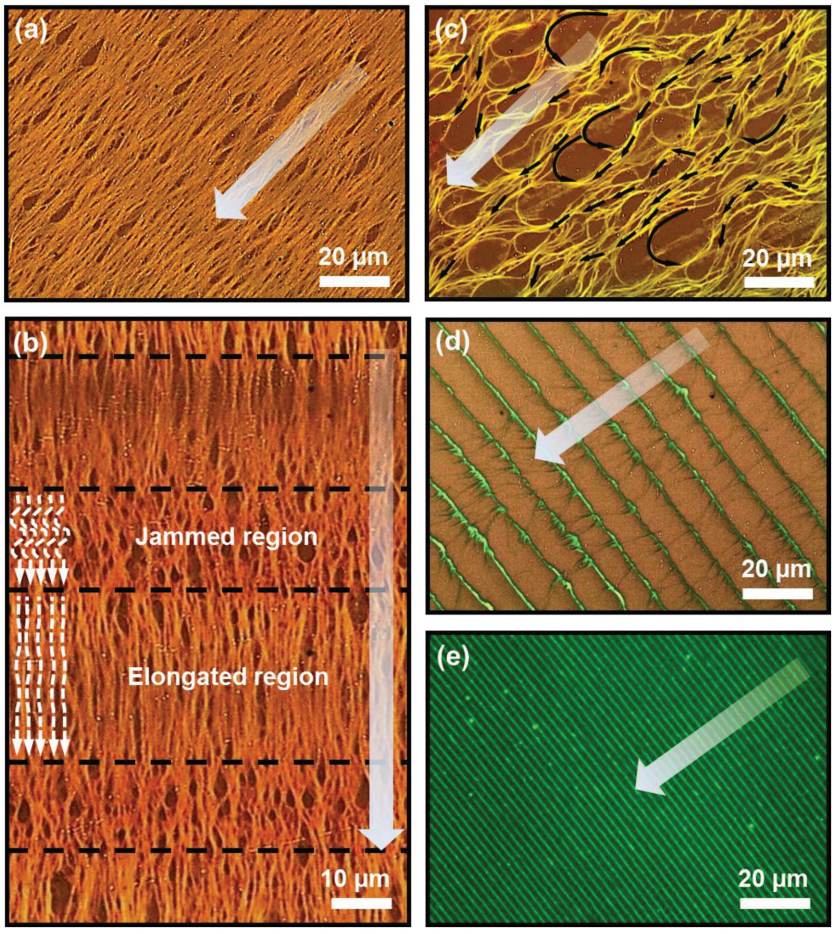

Figure 3. Representative optical micrographs of morphological evolution of DNA nanostructures by changing the concentration of DNA solutions in confined geometry. a) Macroscopically nematic-like ordering of densely packed straight DNA bundles was formed at highly concentrated DNA solution, c = 1000 μg mL^{-1}; continuously textured DNA strands covered the entire substrate surface with the axially symmetric spoke-like configuration toward the contact center. b) Periodically textured DNA pattern formation of slightly jammed and regularly elongated DNA bundled structures at the inner-most site of sphere-on-flat geometry (X_3 region in Figure 1a) with the same DNA concentration in (a). c) The curled and looped DNA strands marked by arrows were observed at the DNA concentration of c = 500 μg mL^{-1}. d) Concentric DNA ring patterns appeared with a large number of branched-DNA filaments interconnected with main rings at the DNA concentration of c = 100 μg mL^{-1}. e) Fluorescent optical microscopy images of a large number of highly regular DNA ring patterns formed with the extremely diluted DNA solution, c = 10 μg mL^{-1} in sphere-on-flat geometry. The white arrows shown in each micrograph indicate the moving direction of the solution front.

regions (Figure 3b). This topological variation of ordered fibril bundles is due presumably to the concentration changes of DNA solution. As the solution front moves inward through the evaporative loss of solvent, the solution volume becomes slowly decreased and thin liquid film of DNA solution recedes deeper toward the contact center since the curvature changes by spherical lens in confined geometry.[24] Subsequently, the DNA spokes may undergo slowly jammed period as more DNAs were bundled to the existing DNA nucleation sites, as shown in Figure 3b. A similar phenomenon has also been observed from other previously reported biological material systems.[43,44] As for the DNA concentration of 500 μg mL^{-1}, DNA bundles were less densely packed and partially lost their orientation as shown in Figure 3c. This optical micrograph shows that DNA bundles tend to form a variety of curled and looped strands following the capillary flow (marked by the arrows in Figure 3c). The weakened alignment of DNA chains can be attributed to the loose intermolecular interaction between DNA chains and the larger capillary force compared to anchoring force (see intermediate DNA concentration in Figure S2, Supporting Information).

With further decrease in the DNA droplet concentration to 100 μg mL^{-1}, concentric ring patterns were first appeared (Figure 3d) due to the cyclic pinning–depinning process at the receding meniscus edges, showing morphological similarity in clear comparison with 50 μg mL^{-1} solution (Figure 2). In the present study, one of the noticeable results is the transition of the DNA arrangement from perpendicular (i.e., spoke-like patterns) to parallel (i.e., coffee ring-like deposition) to the receding contact line by decreasing the solution concentration. Such morphological transitions of the resulting DNA patterns are due presumably to the concentration-dependent variation in the balance between the pinning force of DNA sedimentation and the hydrodynamic dragging force acting on the laterally mobile DNA molecules at the thin film of liquid bridge (i.e., air/water interface); both of these forces are strongly influenced by DNA concentration in solution.[38,32] At a low concentration such as 100 μg mL^{-1}, the amount of DNA deposition at the drying solution front was relatively smaller than high concentration case; fewer solutes were available with which to pin the contact line. On the other hand, the lack of the DNA molecules surrounding the solution at the pinned contact line prohibited the successive growth of DNA bundles and the formation of textured continuous film. As a consequence, limited DNA molecules are accumulated at the edge of contact line for a period of time during the solvent evaporation (i.e., pinning) to reach a critical value before the meniscus is retracted to inward by the interfacial capillary (i.e., depinning), which produce discrete stick–slip motions. It is interesting to note that a large number of DNA filaments that are interconnected with the main periodic rings were shown as an example of the transition stage from DNA-spoke to ring arrays. These fibrillar "branches" of DNA along the main stripe patterns display radial orientation, perpendicular to the moving contact line which covers all the spacing between adjacent stripe patterns (Figures S3 and S4, Supporting Information). Upon further dilution of DNA solution up to 50 μg mL^{-1}, the

small NANO MICRO

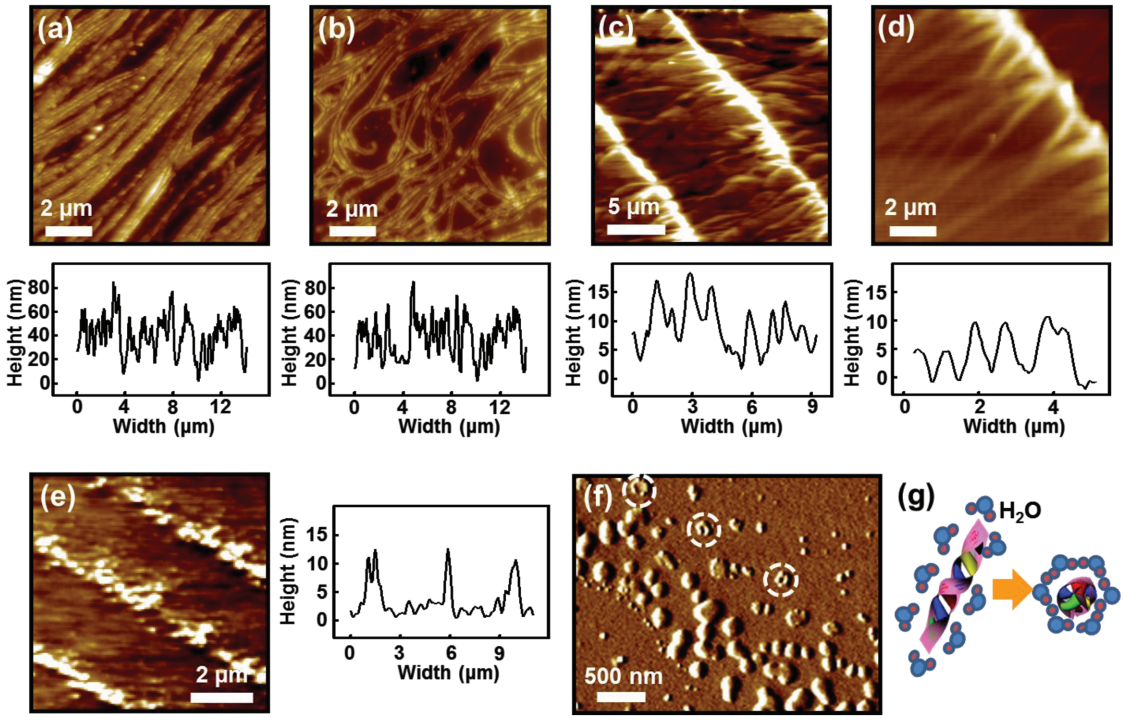

Figure 4. Representative AFM images of DNA surface patterns under different concentration conditions and the corresponding cross-sectional height profiles. a) Straight and densely packed DNA bundles with tens of nanometer scale (c = 1000 μg mL^{-1}). b) The curled and loosely oriented DNA chains (c = 500 μg mL^{-1}). c,d) DNA stripe patterns covered with the branched-DNA filaments between adjacent spacing and zoom-in image (c = 100 μg mL^{-1}). e,f) DNA stripes consist of discontinuous DNA agglomerates and zoom-in image with dotted arrays or nanorings (c = 10 μg mL^{-1}). g) Schematic drawing of hydrated coiled DNA chains forming a cluster.

discrete and well-defined circular patterns were developed (Figure 2a) without the immobilization of DNA branches. Finally, when the concentration of DNA solution decrease as low as 10 μg mL^{-1}, the highly fine and dense DNA ring patterns were obtained with a full surface coverage as shown in Figure 3e and Figure S5 (Supporting Information). To clarify the pattern formation of DNAs, we used a dye molecule (YOYO-1) for fluorescent optical microscope image.

Figure 4 shows AFM height images and the corresponding cross-sectional height profiles of the detailed morphological changes with changing solution concentration. At the high concentration (1000 μg mL^{-1}), it shows straight DNA fibrillar bundles in a radially oriented configuration parallel to the drying direction with tens of nanometer scale. Dilution of the solution to 500 μg mL^{-1} induces the formation of the curled and loosely oriented DNA chains (Figure 4b). As shown in Figure 4c,d (c = 100 μg mL^{-1}), stripe patterns with branched-DNA filaments were observed. Here, the W_{Ring}, H_{Ring}, and H_{Branch} were measured to be 2.02 ± 0.31 μm, 19.4 ± 4 nm, and 13.6 ± 2 nm, respectively. In contrast, in the case of 10 μg mL^{-1} DNA solution, somewhat different morphologies were measured (Figure 4e), which were not immediately noticed by the previous optical microscopy images. As shown in Figure 4f, the zoom-in AFM image clearly reveals that each individual stripe consists of discontinuous DNA agglomerates, which is attributed to the droplet breakup due to the insufficient replenishment of solutes near the drying front, leading to the formation of DNA dotted arrays or nanorings (marked as circles in Figure 4f) via the surface tension driven Rayleigh instability at the pinned contact line that minimized the surface free energy.[25] In addition, at this diluted DNA condition, the hydration of separated DNA chains becomes dominant and thus the hydrated random coiled DNA chains tend to agglomerate to form a cluster at the late stage of water evaporation as schematically described in Figure 4g.[45] The overall observed results of our experiments substantiated that the concentration of the DNA solution in confined geometry is an important factor in determining the characteristics of the assembled DNA shape and stability on the surface (Figure S6, Supporting Information). Conclusively, the competitive advantage of this method is to provide a unique environment such as capillary bridge, toward controlling the motion of moving meniscus within the drying droplet, which, in turn, regulates not only the precise deposition of DNA molecules but also the DNA interchain attractions to form different patterned assemblies.

2.3. DNA Template-Assisted Assembly of CPE

The well-aligned arrays of DNA patterns can be utilized as a template for conjugated polymers, imposing the electrical properties to the defined structures of DNA for further application in electronic devices.[46,47,16,48,49] Negatively charged DNA surfaces are easily modified with positively charged CPEs to form an electrostatic complex in aqueous solution. In this work, we choose a water soluble cationic CPE, poly[9,9-bis(6′-*N,N,N*-trimethylammoniumhexyl)fluorene dibromide],

www.MaterialsViews.com

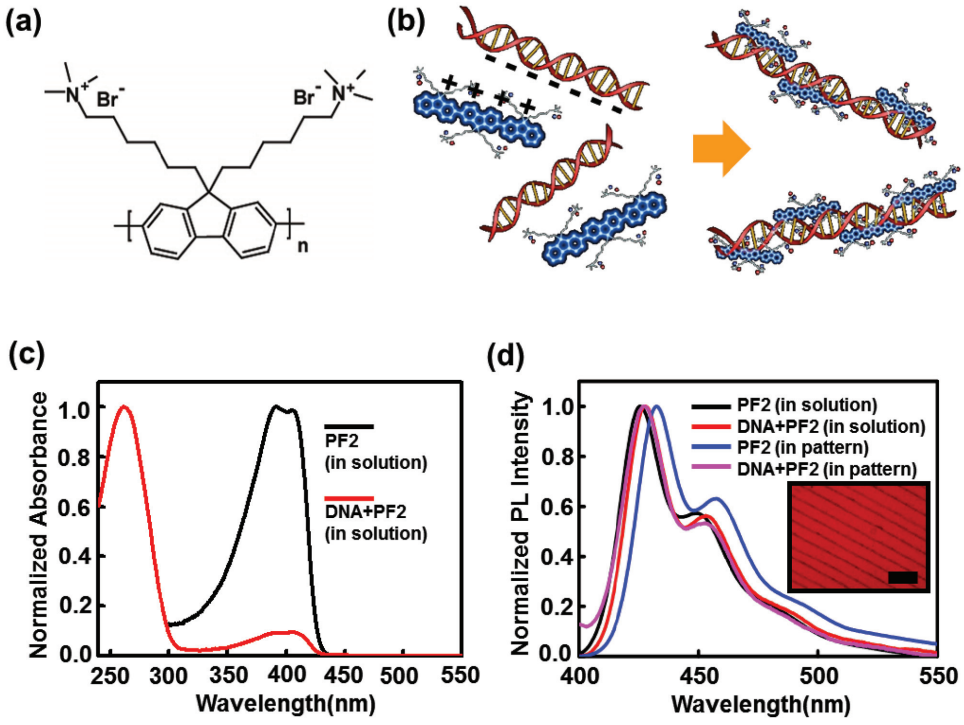

Figure 5. a) Molecular structure of PF2. b) Schematic sketch of electrostatic complexation between DNA and PF2; PF2 chains distributed along DNA chains via complementary charge interactions. c) Normalized UV–vis absorption spectra of PF2 and DNA/PF2 complex in water. d) PL spectra of PF2 in the presence and absence of DNA in water and in pattern (inset: optical micrograph of highly ordered arrays of DNA/PF2; scale bar = 10 μm).

(PF2, M_n = 15 000 g mol^{-1}, PDI = 2.57) as a model system to coat the individual DNA surfaces forming electrostatic complexation in an aqueous solution.[34–36] **Figure 5**a shows a chemical structure of PF2 which is composed of the backbone of polyfluorene with cationic trimethylammoniumhexyl side chains. A schematic illustration of forming the complex is displayed in Figure 5b, which is involved with continuous decoration of CPEs on the surface of DNA fibrils via electrostatic attractions. We measured the UV–vis absorption and photoluminescence (PL) spectra for PF2 and DNA/PF2 complexes in water and in patterned film (Figure 5c,d). The DNA/PF2 complex in water (20:1 concentration ratio of DNA to PF2) shows two absorption peaks at 390 and 260 nm that originate from PF2 and DNA, respectively. The PL maximum (λ_{PL}) of PF2 was measured at 426 nm in water and at 432 nm in patterned film, clearly showing a redshift in film due to increased effective π-conjugation via interchain aggregation of PF2 in a solid state. In the case of the DNA/PF2 mixture in aqueous solution, the PL spectrum shows λ_{PL} = 428 nm which is similar to that of PF2 in water, suggesting that electrostatic complexation with DNA does not disturb the electronic structure of PF2. Interestingly, almost identical PL spectra were measured for the DNA/PF2 mixture in solutions and solid states (electrostatic complex of PF2 on the patterned DNA), indicating negligible interchain aggregation of PF2 by electrostatic complexation with DNA (see λ_{PL} = 432 nm for PF2 in film). It would be acknowledged that DNAs may interrupt the polymer–polymer interchain aggregation, thereby inducing a stretched polymeric chain via electrostatic complexation on the patterned DNA arrays.[33,48] The DNA/PF2 complexes were tethered on a substrate with highly aligned configuration through droplet evaporation in a unique geometry (i.e., sphere-on-flat) with optimized concentration, c = 100 μg mL^{-1} (inset image in Figure 5, see details in the Experimental Section).

The use of highly aligned DNA-templated conjugated polymers as electrically conductive channels is of great interest in device construction, such as positioning the DNA patterns with electrode arrays. **Figure 6**a shows a schematic illustration of a fabrication process for two terminal devices using a shadow mask. In the device fabrication process, a major technical challenge was the integration of the aligned nanoscale patterns onto the desired locations of electrodes (i.e., electrical channel between electrical bridges), which was performed using a micropositioner under an optical microscope for the precision alignment. Then, the metal electrodes were deposited by thermal evaporation of aluminum (200 nm thick) in a high vacuum chamber. The metal layers on top of DNA-templated PF2 nanowires were electrically isolated (right panel in Figure 6a), which enables the current measurements on multichannel devices of each PF2 and DNA-templated PF2 nanowires. Figure 6b shows a representative channel region in the optical microscope image between two electrodes; the width and separations of the Al electrodes were 50 and 25 μm, respectively; the integrated individual electrically conductive channels (i.e., individual DNA/PF2 nanowires) were conformally wrapped by the overlying metal electrodes. It is noteworthy that the DNA-templated PF2 nanowires maintain excellent alignment throughout the process without any degradation. The width and height of such nanowires between two electrodes were measured to be 1.5 ± 0.19 μm and 18.7 ± 3 nm, respectively

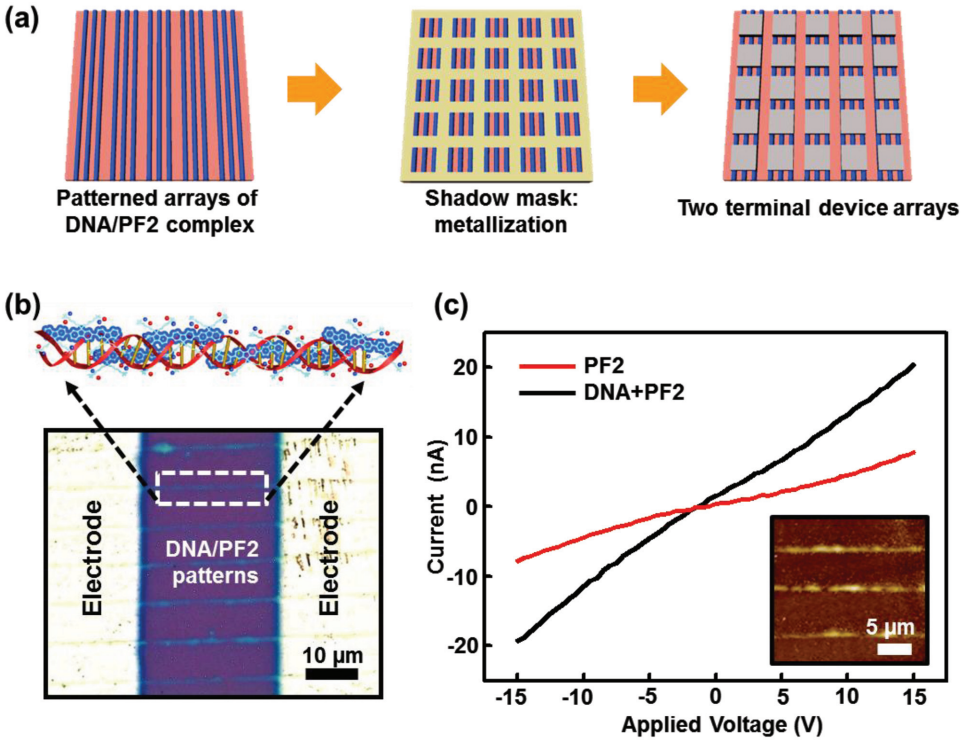

Figure 6. a) Schematic diagram of a fabrication process of DNA-templated devices; metallization was performed with the precise alignment of a shadow mask on patterned nanowire arrays of DNA/PF2 complex. b) Optical micrograph of a pair of Al electrodes on aligned DNA/PF2 arrays on a Si/SiO_2 substrate. c) Current–voltage (*I–V*) characteristics; linear fits define the effective resistance. The inset shows the AFM image of patterned nanowire arrays of DNA/PF2.

(inset AFM image in Figure 6c). Finally, the electrical characteristics measured in ambient condition are presented in Figure 6c. The associated current–voltage (*I–V*) curves yield the successful electrical responses of the DNA-templated PF2 nanowires. The current levels measured from devices built with DNA-templated PF2 nanowires are approximately two times higher than that of the PF2 nanowire itself (without the DNA template), for both positive and negative bias cases. The typical values of recorded conductance for the DNA-templated PF2 nanowires were 11–14 pS, which is comparable to the reported values.[50] This large increase in conductivity can be primarily attributed to the aligned or stretched conjugated polymer chains (PF2) along the DNA strands,[48] supported by the previously reported direction-dependent conductivity enhancement of the DNA and conjugated polymer complexes.[35]

3. Conclusion

In summary, we developed a simple yet robust evaporative self-assembly strategy for creating highly regular DNA arrays over large area (i.e., millimeter scale) by allowing a drop of DNA solution to dry in sphere-on-flat geometry. This geometrical configuration provides a unique environment for controlling DNA to flow within the evaporating droplet, thereby precisely regulates the anchoring of DNA solutes on a substrate in a remarkably controllable, cost-effective, and reproducible manner. Subsequently, by varying the concentration of DNA solutions, either fibrous textured nanostructures or high density of patterned DNA nanowires was formed on the Si/SiO_2 substrates. More interestingly, by subjecting the solution composed of the complex of DNA and PF2 to evaporate in sphere-on-flat geometry, highly ordered DNA/PF2 patterns were formed and utilized as templates to fabricate two terminal device arrays. We envision that the ability to modify DNA molecules (e.g., complexation with CPE) and deposit them in a controllable manner (i.e., possessing desirable spatial arrangement) may provide opportunities to realize the potential of DNA-based nanotechnology for more advanced molecular nanoelectronic devices and transducing elements in chemical sensors.[37,51,16]

4. Experimental Section

Preparation of Salmon Sperm DNA Solution: To prepare the DNA solution, salmon sperm DNA (≈2000 bp, Sigma-Aldrich) was used as supplied without further purification. Dried DNA powder (10 mg) was placed in a 15 mL Falcon tube, and then DI water (10 mL) was added to yield a concentration of 1000 μg mL^{-1}. Next, the solution was heated for 24 h at 80 °C to dissolve DNA completely, and then it was treated by ultrasonication for 20 min. Series of DNA solutions were prepared by dilution to yield the desired concentration ranging from 500 to 10 μg mL^{-1}. All the prepared DNA solutions were vigorously stirred by using a vortex mixer for 15 min just before use.

Sphere-On-Fat Confined Geometry: A spherical lens (R = 10.94 mm, D = 10.15 mm) made of fused silica and Si/SiO_2 wafer was used as the upper and lower surfaces, respectively, to

construct a confined geometry, i.e., the sphere-on-flat geometry. The lens and substrates were cleaned with a mixture of hydrogen peroxide and sulfuric acid (0.3/0.7 by volume), rinsed with DI water, and dried by blowing nitrogen gas. The contact of the lens with Si/SiO_2 was made using a micropositioning stage with a lens holder, and then the aqueous DNA droplet (25 μL) was loaded in between the two surfaces, then the upper spherical lens was slowly brought into contact with the lower stationary flat substrate (Figure 1a). All procedures were conducted in a sealed chamber to maintain constant temperature (≈30 °C) during the evaporation process.

Synthesis of Poly[9,9-bis(6′-bromohexyl)fluorene] (n-PF2): The neutral polyfluorene precursor was synthesized by following the previously reported procedure.[52] The ^1H NMR spectra were recorded on a Bruker AVANCE 400 spectrometer, with tetramethylsilane as the internal reference. A mixture of 2,7-bis(4,4,5,5-tetramethyl-1,3,2-dioxaborolan-2-yl)-9,9-bis(6′-bromohexyl)fluorene (0.220 g, 0.301 mmol), 2,7-dibromo-9,9-bis(6′-bromohexyl)fluorene (0.196 g, 0.301 mmol), and $(PPh_3)_4Pd$ was added in a round bottom flask in a dry box. Degassed toluene (8 mL), aqueous 2 M K_2CO_3 (4 mL) solution, and phase transfer catalyst Aliquat 336 were transferred to the above flask. After stirring the reaction solution at 85 °C for 24 h, bromobenzene (5 mg, 0.03 mmol in 1 mL toluene) as an end capper was added and stirred at 85 °C for 12 h. The reaction mixture was cooled to room temperature and added slowly to a viscously stirred methanol (200 mL). The polymer was collected by filtration and purified by Soxhlet extraction with acetone to remove oligomers and catalyst residues. The final product, a white polymer, was obtained after drying under vacuum. Yield: 71% (210 mg), ^1H NMR (400 MHz, $CDCl_3$, δ): 8.12–7.86 (m, 6H), 3.28 (m, 4H), 2.10 (m, 4H), 1.68 (m, 4H), 1.30–1.12 (m, 8H), 0.89–0.75 (m, 4H).

Synthesis of Poly[9,9-bis(6′-N,N,N-trimethylammoniumhexyl)-fluorene Dibromide] (PF2): Cationic water-soluble PF2 was obtained through a simple quaternization reaction.[53] Condensed trimethylamine (3–5 mL) was added dropwise to a solution of neutral precursor polymer (n-PF2, 100 mg) in tetrahydrofuran (10 mL) at −78 °C. The mixture was allowed to warm up to room temperature gradually. The precipitate was redissolved by addition of excess methanol and additional 2 mL trimethylamine was added at −78 °C. The resulting mixture was stirred for 24 h at room temperature. After removal of solvents under reduced pressure, PF2 was precipitated by adding the concentrated polymer solution dropwise into acetone. The final cationic PF2 was then collected and dried in a vacuum oven. Yield: 87% (108 mg), ^1H NMR (400 MHz, DMSO-d_6, δ): 8.27–7.96 (m, 6H), 3.35 (m, 4H), 3.19 (br, 4H), 2.96 (s, 18H), 1.54 (br, 4H), 1.15 (br, 8H), 0.83 (br, 4H).

Preparation of Salmon Sperm DNA/PF2 Complex: The DNA/PF2 complex in an aqueous solution was prepared by mixing 20:1 concentration ratio of DNA to PF2 in water, inducing the complemental electrostatic interaction between the backbone of polyfluorene with cationic trimethylammoniumhexyl side chains and the anionic phosphate backbone of DNA. For more information, the stoichiometric ratio (PF2:phosphate) was approximately estimated in the complex as follows. Because the number average molecular weight of salmon sperm DNA (≈2000 bp) was determined to be 1.3×10^6 g mol^{-1},[54] the prepared solution in confined geometry was composed of [DNA] = 100 μg mL^{-1} = 7.69×10^{-8} M and [PF2] = 5 μg mL^{-1} = 1.1×10^{-5} M (per repeat unit) for the evaporative self-assembly. Each phosphate group in DNA contains one negative charge (total [– charges] per single DNA chain = −2000), while PF2 has two positive charges per repeating unit. The resulting DNA/PF2 complex possesses [–] = 1.54×10^{-4} M and [+] = 2.2×10^{-5} M, with a charge ratio of [–]/[+] = 7.

Characterization: Optical microscopy (Olympus BX51) was performed in the reflective mode, and AFM imaging of DNA patterns with different dimensions was obtained by using a scanning force microscope (Park Systems, XE-100) in noncontact mode. To measure electrical characteristics of DNA/CPE patterns, Al electrodes were deposited by thermal evaporation of aluminum (≈200 nm) in a high vacuum chamber. Prior to the evaporation step, the shadow mask was aligned on a fixed substrate using a micropositioner under an optical microscope. Finally, the measurement of electrical properties was carried out using a probe station with a semiconductor parameter analyzer (Agilent 4145b) in ambient condition.

Supporting Information

Supporting Information is available from the Wiley Online Library or from the author.

Acknowledgements

D.G.B. and J.-E.J. contributed equally to this work. This work was supported by the National Research Foundation of Korea Grant funded by the Korean Government (NRF-2014R1A1A2058350 and 2015R1A2A1A15055605).

[1] G. M. Whitesides, B. Grzybowski, *Science* **2002**, *295*, 418.
[2] S. Zhang, *Nat. Biotechnol.* **2003**, *21*, 1171.
[3] S. I. Stupp, *Nano Lett.* **2010**, *10*, 4783.
[4] H. Gu, J. Chao, S.-J. Xiao, N. C. Seeman, *Nat. Nanotechnol.* **2009**, *4*, 245.
[5] K. Keren, R. S. Berman, E. Buchstab, U. Sivan, E. Braun, *Science* **2003**, *302*, 1380.
[6] Y. Ma, J. Zhang, G. Zhang, H. He, *J. Am. Chem. Soc.* **2004**, *9*, 7097.
[7] P. Björk, A. Herland, I. G. Scheblykin, O. Inganäs, *Nano Lett.* **2005**, *5*, 1948.
[8] H. A. Becerril, A. T. Woolley, *Chem. Soc. Rev.* **2009**, *38*, 329.
[9] F. A. Aldaye, A. L. Palmer, H. F. Sleiman, *Science* **2008**, *321*, 1795.
[10] H. Yokota, F. Johnson, H. Lu, R. M. Robinson, A. M. Belu, M. D. Garrison, B. D. Ratner, B. J. Trask, D. L. Miller, *Nucleic Acids Res.* **1997**, *25*, 1064.
[11] E. Auyeung, J. I. Cutler, R. J. Macfarlane, M. R. Jones, J. Wu, G. Liu, K. Zhang, K. D. Osberg, C. A. Mirkin, *Nat. Nanotechnol.* **2011**, *7*, 24.
[12] M. Pillers, V. Goss, M. Lieberman, *Acc. Chem. Res.* **2014**, *47*, 1759.
[13] C. Lin, Y. Ke, Y. Liu, M. Mertig, J. Gu, H. Yan, *Angew. Chem. Int. Ed.* **2007**, *46*, 6089.
[14] R. Hassanien, M. Al-Hinai, S. A. Farha Al-Said, R. Little, L. Šiller, N. G. Wright, A. Houlton, B. R. Horrocks, *ACS Nano* **2010**, *4*, 2149.
[15] J. Choi, H. Chen, F. Li, L. Yang, S. S. Kim, R. R. Naik, P. D. Ye, J. H. Choi, *Small* **2015**, *11*, 5520.

[16] A. Houlton, A. R. Pike, M. A. Galindo, B. R. Horrocks, *Chem. Commun.* **2009**, 1797.
[17] S. H. Kang, W. S. Hwang, Z. Lin, S.-H. Kwon, S. W. Hong, *Nano Lett.* **2015**, *15*, 7913.
[18] A. N. Sokolov, F. L. Yap, N. Liu, K. Kim, L. Ci, O. B. Johnson, H. Wang, M. Vosgueritchian, A. L. Koh, J. Chen, J. Park, Z. Bao, *Nat. Commun.* **2013**, *4*, 2402.
[19] X. Michalet, R. Ekong, F. Fougerousse, S. Rousseaux, C. Schurra, N. Hornigold, M. v. Slegtenhorst, J. Wolfe, S. Povey, J. S. Beckmann, A. Bensimon, *Science* **1997**, *277*, 1518.
[20] F. Dewarrat, M. Calame, C. Schönenberger, *Single Mol.* **2002**, *3*, 189.
[21] C. A. P. Petit, J. D. Carbeck, *Nano Lett.* **2003**, *3*, 1141.
[22] J. Guan, L. J. Lee, *Proc. Natl. Acad. Sci. USA* **2005**, *102*, 18321.
[23] A. Cerf, T. Alava, R. A. Barton, H. G. Craighead, *Nano Lett.* **2011**, *11*, 4232.
[24] S. W. Hong, J. Xia, Z. Lin, *Adv. Mater.* **2007**, *19*, 1413.
[25] S. W. Hong, J. Xu, J. Xia, Z. Lin, F. Qiu, Y. Yang, *Chem. Mater.* **2005**, *17*, 6223.
[26] S. W. Hong, M. Byun, Z. Lin, *Angew. Chem. Int. Ed.* **2009**, *121*, 520.
[27] S. W. Hong, J. Wang, Z. Lin, *Angew. Chem. Int. Ed.* **2009**, *121*, 8506.
[28] R. D. Deegan, O. Bakajin, T. F. Dupont, G. Huber, S. R. Nagel, T. A. Witten, *Nature* **1997**, *389*, 827.
[29] E. Adachi, A. S. Dimitrov, K. Nagayama, *Langmuir* **1995**, *11*, 1057.
[30] R. G. Larson, *Angew. Chem. Int. Ed.* **2012**, *51*, 2546.
[31] W. Han, Z. Lin, *Angew. Chem. Int. Ed.* **2012**, *51*, 1534.
[32] L. Frastia, A. J. Archer, U. Thiele, *Phys. Rev. Lett.* **2011**, *106*, 077801.
[33] P. Björk, D. Thomsson, O. Mirzov, J. Wigenius, O. Inganäs, I. G. Scheblykin, *Small* **2008**, *5*, 96.
[34] S. M. D. Watson, A. R. Pike, J. Pate, A. Houlton, B. R. Horrocks, *Nanoscale* **2014**, *6*, 4027.
[35] P. Björk, A. Herland, M. Hamedi, O. Inganäs, *J. Mater. Chem.* **2010**, *20*, 2269.
[36] M. Hamedi, A. Elfwing, R. Gabrielsson, O. Inganäs, *Small* **2012**, *9*, 363.
[37] Y. W. Kwon, C. H. Lee, D. H. Choi, J. I. Jin, *J. Mater. Chem.* **2009**, *19*, 1353.
[38] J. Xu, J. Xia, S. W. Hong, Z. Lin, F. Qiu, Y. Yang, *Phys. Rev. Lett.* **2006**, *96*, 066104.
[39] M. Byun, W. Han, B. Li, S. W. Hong, J. Cho, Q. Zou, Z. Lin, *Small* **2015**, *12*, 1641.
[40] J. Huang, F. Kim, A. R. Tao, S. Connor, P. Yang, *Nat. Mater.* **2005**, *4*, 896.
[41] C. Farcau, H. Moreira, B. Viallet, J. Grisolia, L. Ressier, *ACS Nano* **2010**, *4*, 7275.
[42] H. Ko, S. Peleshanko, V. V. Tsukruk, *J. Phys. Chem. B* **2004**, *108*, 4385.
[43] W.-J. Chung, J.-W. Oh, K. W. Kwak, B. Y. Lee, J. Meyer, E. Wang, A. Hexemer, S.-W. Lee, *Nature* **2011**, *478*, 364.
[44] Y. Lin, E. Balizan, L. A. Lee, Z. Niu, Q. Wang, *Angew. Chem. Int. Ed.* **2010**, *49*, 868.
[45] X. Fang, B. Li, E. Petersen, Y. S. Seo, V. A. Samuilov, Y. Chen, J. C. Sokolov, C. Y. Shew, M. H. Rafailovich, *Langmuir* **2006**, *22*, 6308.
[46] M. Taniguchi, T. Kawai, *Physica E* **2006**, *33*, 1.
[47] S. Pruneanu, S. A. Farha Al-Said, L. Dong, T. A. Hollis, M. A. Galindo, N. G. Wright, A. Houlton, B. R. Horrocks, *Adv. Funct. Mater.* **2008**, *18*, 2444.
[48] S. M. D. Watson, M. A. Galindo, B. R. Horrocks, A. Houlton, *J. Am. Chem. Soc.* **2014**, *136*, 6649.
[49] S. M. D. Watson, A. Houlton, B. R. Horrocks, *Nanotechnology* **2012**, *23*, 505603.
[50] P. Nickels, W. U. Dittmer, S. Beyer, J. P. Kotthaus, F. C. Simmel, *Nanotechnology* **2004**, *15*, 1524.
[51] G. Wang, H. Tanaka, L. Hong, Y. Matsuo, K. Niikura, M. Abe, K. Matsumoto, T. Ogawa, K. Ijiro, *J. Mater. Chem.* **2012**, *22*, 13691.
[52] R. Yang, H. Wu, Y. Cao, G. C. Bazan, *J. Am. Chem. Soc.* **2006**, *128*, 14422.
[53] H.Y. Woo, D. Vak, D. Korystov, A. Mikhailovsky, G. C. Bazan, D.-Y. Kim, *Adv. Mater.* **2007**, *17*, 290.
[54] K. Tanaka, Y. Okahata, *J. Am. Chem. Soc.* **1996**, *118*, 10679.

Received: April 19, 2016
Revised: May 24, 2016
Published online: June 28, 2016